Molecular Therapy
Nucleic Acids
Original Article

hsa_circ_0068631 promotes breast cancer progression through c-Myc by binding to EIF4A3

Xuehui Wang,[1,2,3] Minghui Chen,[1,3] and Lin Fang[1,2]

[1]Shanghai Tenth People's Hospital, School of Medicine, Tongji University, Shanghai 200072, China; [2]Clinical Medical College of Shanghai Tenth People's Hospital, Nanjing Medical University, Nanjing 211166, China

Breast cancer (BC) is one of the most common malignancies among women worldwide with a high incidence of recurrence and metastasis. In this study, we demonstrate that hsa_circ_0068631, a circRNA generated from the transferrin receptor (TFRC), is upregulated in BC tissues and cell lines. Knockdown of hsa_circ_0068631 inhibited the proliferation and migration of BC cells *in vitro* and *in vivo*. Mechanistically, an RNA pull-down assay and RNA immunoprecipitation assay revealed that eukaryotic translation initiation factor 4A3 (EIF4A3) could bind to hsa_circ_0068631 and c-Myc mRNA. Additionally, the expression of hsa_circ_0068631 was positively correlated with c-Myc, and the upregulation of hsa_circ_0068631 was a crucial factor for the dysregulation of c-Myc. Through an actinomycin D assay, we confirmed that the mRNA stability of c-Myc was influenced by hsa_circ_0068631 and EIF4A3. Furthermore, hsa_circ_0068631 could recruit EIF4A3 to increase c-Myc mRNA stability. Rescue assays manifesting depletion of c-Myc rescued the promotive effect of hsa_circ_0068631 overexpression on biological activities in BC. In conclusion, to our knowledge, this study is the first to unveil the role of hsa_circ_0068631 and the hsa_circ_0068631/EIF4A3/c-Myc axis in BC, providing a new target for BC treatment.

INTRODUCTION

Breast cancer (BC), known as one of the most common malignancies among women worldwide, is a serious threat to human survival and health.[1,2] Although significant advances in the diagnosis and treatment of BC have been achieved in the past few years, the mortality rates for BC are still high due to the high incidence of recurrence and metastasis. Therefore, in-depth investigations focusing on the potential molecular mechanisms in BC are urgently needed.

Circular RNAs (circRNAs), characterized by a closed and continuous loop structure without a 5′ cap or a 3′ poly(A) tail, are involved in pathological processes of multiple malignancies.[3] Previous studies have proven that circRNAs participate in various pathways related to BC tumorigenesis. For example, hsa_circ_0001667 promoted BC cell proliferation and survival via regulating the Hippo pathway.[4] hsa_circ_001569 could promote BC cell proliferation and metastasis by modulating the phosphatidylinositol 3-kinase (PI3K)/AKT pathway.[5] Importantly, compared with conventional linear RNAs, circRNAs are more stable in tissues, blood, and exosomes, indicating that circRNAs have a promising potential as diagnostic and therapeutic biomarkers in BC.[6–8]

In recent years, the BC 21-gene assay provides important references for the prognosis, recurrence, and drug selection of BC.[9] Transferrin receptor (TFRC) was verified as a valuable endogenous control gene in the BC 21-gene assay.[10,11] We selected hsa_circ_0068631, which was produced at the TFRC gene, for our study. In our current study, we found that hsa_circ_0068631 was highly expressed in BC tissues and cell lines. The functional investigation showed that hsa_circ_0068631 could accelerate BC progression *in vivo* and *in vitro*. Through bioinformatics analysis and mechanism investigations, we verified that hsa_circ_0068631 could maintain c-Myc mRNA stability and positively regulate c-Myc by binding to eukaryotic translation initiation factor 4A3 (EIF4A3), thereby providing potential therapeutic targets in BC treatment.

RESULTS

hsa_circ_0068631 is highly expressed in BC tissues and cell lines

hsa_circ_0068631, formed by circularization of exons 2–3 of the gene TFRC, was located at chromosome 3:195802029–195803993 according to the UCSC Genome Browser (http://genome.ucsc.edu/). Sanger sequencing was performed to verify the back-splicing junction site of exon 3 toward exon 2 of hsa_circ_0068631 (Figure 1A). The existence of hsa_circ_0068631 PCR products was further verified by 1% agarose gel electrophoresis. Additionally, knockdown and overexpression of hsa_circ_0068631 were carried out to prove the specificity of the band (Figure 1B). An RNase R resistant assay was performed to confirm that the hsa_circ_0068631 is circular. The results showed that RNase R could digest linear TFRC RNA but not hsa_circ_0068631 (Figures 1C and 1D). Then, we conducted an actinomycin D (ActD) assay in MDA-MB-231 and MCF-7 cells and results showed that hsa_circ_0068631 rather than TFRC could resist actinomycin D, indicating that hsa_circ_0068631 was more stable and has a longer half-life (Figures 1E and 1F). To explore the cellular

Received 2 March 2021; accepted 2 July 2021;
https://doi.org/10.1016/j.omtn.2021.07.003.

[3]These authors contributed equally

Correspondence: Lin Fang, Shanghai Tenth People's Hospital, School of Medicine, Tongji University, Shanghai 200072, China.
E-mail: fanglin2017@126.com

 © 2021 The Author(s).
This is an open access article under the CC BY-NC-ND license (http://creativecommons.org/licenses/by-nc-nd/4.0/).

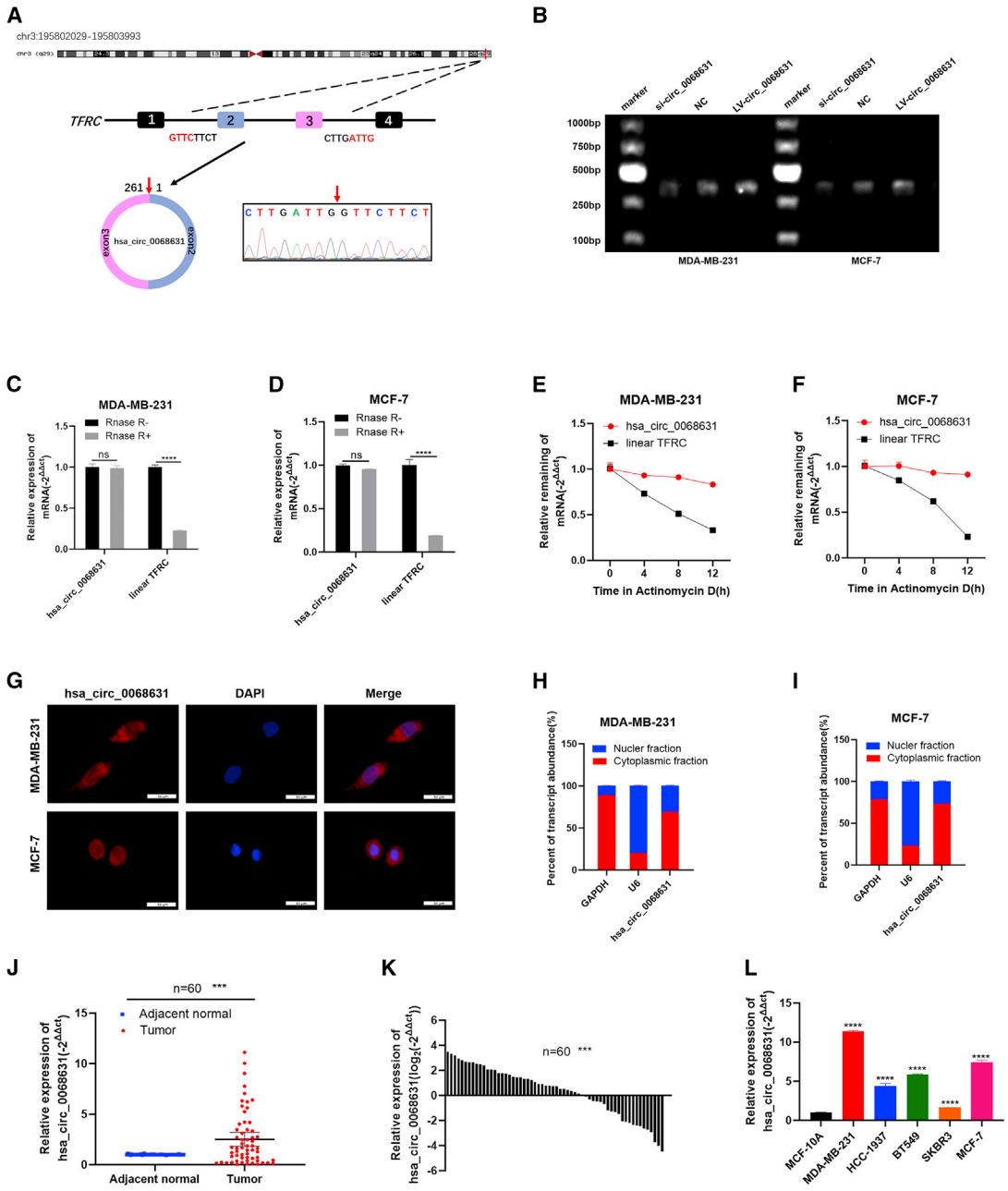

Figure 1. hsa_circ_0068631 was highly expressed in BC tissues and cell lines

(A) hsa_circ_0068631 is formed by circularization of exons 2–3 of the gene TFRC, and the back-splicing junction site was verified by Sanger sequencing. (B) Existence of hsa_circ_0068631 in BC cells was verified by agarose gel electrophoresis. (C and D) Quantitative real-time PCR analysis of hsa_circ_0068631 and linear TFRC in BC cells treated with RNase R. (E and F) After actinomycin D treatment, the mRNA stability of hsa_circ_0068631 and TFRC in BC cells was determined by quantitative real-time PCR. (G) RNA FISH for hsa_circ_0068631 and nuclei were stained with DAPI (scale bars, 50 μm). Red shows hsa_circ_0068631; blue shows DAPI. (H and I) Expression levels of the cytoplasmic control (GAPDH), the nuclear control (U6), and hsa_circ_0068631 were determined by quantitative real-time PCR in the cytoplasmic and nuclear fractions of BC cells. (J and K) hsa_circ_0068631 was highly expressed in tumor tissues compared with adjacent normal tissues. (L) hsa_circ_0068631 was highly expressed in BC cells compared with MCF-10A cells. ***$p < 0.001$, ****$p < 0.0001$.

distribution of hsa_circ_0068631, a fluorescence *in situ* hybridization (FISH) analysis was performed and revealed that most of the hsa_circ_0068631 was located in the cytoplasm (Figure 1G). Consistently, we confirmed that hsa_circ_0068631 was enriched in the cytoplasm of BC cells by quantitative real-time PCR in the cytoplasmic and nuclear fractions (Figures 1H and 1I). hsa_circ_0068631 expression in BC was

Table 1. The relationship between the expression of hsa_circ_0068631 and various clinicopathological variables in BC patients

		hsa_circ_0068631 expression		
Patient characteristics	Total	High (n = 39)	Low (n = 21)	p Value
Age				0.4302
<60	27	19	8	
≥60	33	20	13	
TNM stage				0.0136*
I/II	39	21	18	
III/IV	21	18	3	
Tumor size (cm)				0.0276*
≤2	44	25	19	
>2	16	14	2	
Lymph node metastasis				0.0083**
Negative	38	20	18	
Positive	22	19	3	
Distant metastasis				0.0258*
No	52	31	21	
Yes	8	8	0	

*p < 0.05.
**p < 0.01.

evaluated by quantitative real-time PCR. As shown in Figures 1J and 1K, the expression of hsa_circ_0068631 was significantly elevated in BC tissues (39/60, 65%) compared with adjacent normal tissues. Consistently, five BC cell lines (MDA-MB-231, MCF-7, HCC-1937, BT549, and SKBR3) presented higher hsa_circ_0068631 expression compared with MCF-10A cells (Figure 1L). Then, MDA-MB-231 and MCF-7 cells were chosen for subsequent experiments due to results discussed above. To better identify the role of hsa_circ_0068631 in BC, we analyzed the relationship between hsa_circ_0068631 expression and the clinical and pathological variables in 60 BC patients. High expression of hsa_circ_0068631 was positively associated with tumor-lymph node-metastasis (TNM) stage, tumor size, lymph node metastasis and distant metastasis, but it had no correlation with age (Table 1).

hsa_circ_0068631 exerts an oncogenic role in BC cells

High expression of hsa_circ_0068631 indicated its oncogenic role in BC. hsa_circ_0068631 was knocked down in MDA-MB-231 and MCF-7 cell lines using small interfering RNA (siRNA) targeting human hsa_circ_0068631 (si-circ_0068631). According to the transfection efficiency verified by quantitative real-time PCR, we chose si-circ_0068631-1 for further study (Figure 2A). Meanwhile, we stably overexpressed hsa_circ_0068631 in BC cells using lentivirus plasmids targeting human hsa_circ_0068631 (LV-circ_0068631) and empty vector (LV-vector) as a control (Figure 2B). The MTT (3-(4,5-dimethylthiazol-2-yl)-2,5-diphenyltetrazolium bromide) assay and colony formation assay were performed to detect cell viability, and the results showed that cell proliferation was clearly promoted by hsa_circ_0068631 (Figures 2C–2G). Meanwhile, a transwell migration assay and wound-healing assay illustrated that the capabilities of BC cell migration were suppressed in the hsa_circ_0068631-depletion group whereas they were promoted in the hsa_circ_0068631-overexpression group (Figures 2H and 2I; Figures S1A and S1B). In addition, cell cycle was further tested by flow cytometry analysis, indicating that hsa_circ_0068631 depletion increased the percentage of the G_0/G_1 phase of BC cells (Figures 2J and 2L). Also, hsa_circ_0068631 overexpression decreased the percentage of the G_0/G_1 phase of BC cells (Figures 2K and 2M). All results above proved that hsa_circ_0068631 plays an oncogenic role in BC cells.

hsa_circ_0068631 could bind to EIF4A3

Since hsa_circ_0068631 was generated from the gene TFRC, we first investigated whether hsa_circ_0068631 affected its expression. The results showed that there was no significant change in mRNA and protein level of TFRC after knockdown and overexpression of circ_0068631, indicating that hsa_circ_0068631 exerts its roles independent of its parent gene (Figures S1C–S1E). According to the prediction of CircInteractome (https://circinteractome.nia.nih.gov/), hsa_circ_0068631 had a binding site with an EIF4A3 matching circRNA junction, indicating that hsa_circ_0068631 has protein-binding capacity (Figure 3A). To verify whether hsa_circ_0068631 could bind to RNA-binding protein (RBP), an RNA pull-down silver staining assay was performed. As shown in Figure 3B, specific bands were shown at 40–70 kDa, indicating that there are some RBPs that could bind to hsa_circ_0068631. Then, the interaction between EIF4A3 and hsa_circ_0068631 was further validated by RNA pull-down, followed by a western blotting assay (Figure 3C). In addition, an RNA immunoprecipitation (RIP) assay further confirmed the enrichment of hsa_circ_0068631 in the anti-EIF4A3 group compared with the anti-immunoglobulin G (IgG) group (Figures 3D and 3E). Moreover, an immunofluorescence (IF)/FISH assay showed that hsa_circ_0068631was co-located with EIF4A3 in BC cells (Figure 3F). Taken together, these data demonstrated that hsa_circ_0068631 could bind to EIF4A3. We found that EIF4A3 was highly expressed in BC tissues in The Cancer Genome Atlas (TCGA) database (Figure S1F). In addition, we tested the EIF4A3 protein level in BC cell lines and discovered the high expression of EIF4A3 in BC cell lines (Figure 4A). Then, we respectively knocked down and overexpressed EIF4A3 in BC cells, and the efficiency was confirmed in both mRNA and protein levels (Figures 4B–4E). Consistent with its expression pattern, EIF4A3 depletion remarkably inhibited BC cell proliferation and migration, while overexpression of EIF4A3 exerted oncogenic activities in BC cells (Figures 4F–4L; Figures S1G and S1H). Next, we investigated whether hsa_circ_0068631 affected the expression of EIF4A3, but we detected no significant changes in both mRNA or protein levels of EIF4A3 with hsa_circ_0068631 depletion or overexpression (Figures 4M–4O). Thus, we proposed a hypothesis that hsa_circ_0068631 might regulate downstream mRNAs via recruiting and binding to EIF4A3.

hsa_circ_0068631 regulates c-Myc through recruiting EIF4A3 at the post-transcriptional level

According to systematic analysis of the co-expression network of EIF4A3 in cancers, the biological pathway showed that the c-Myc

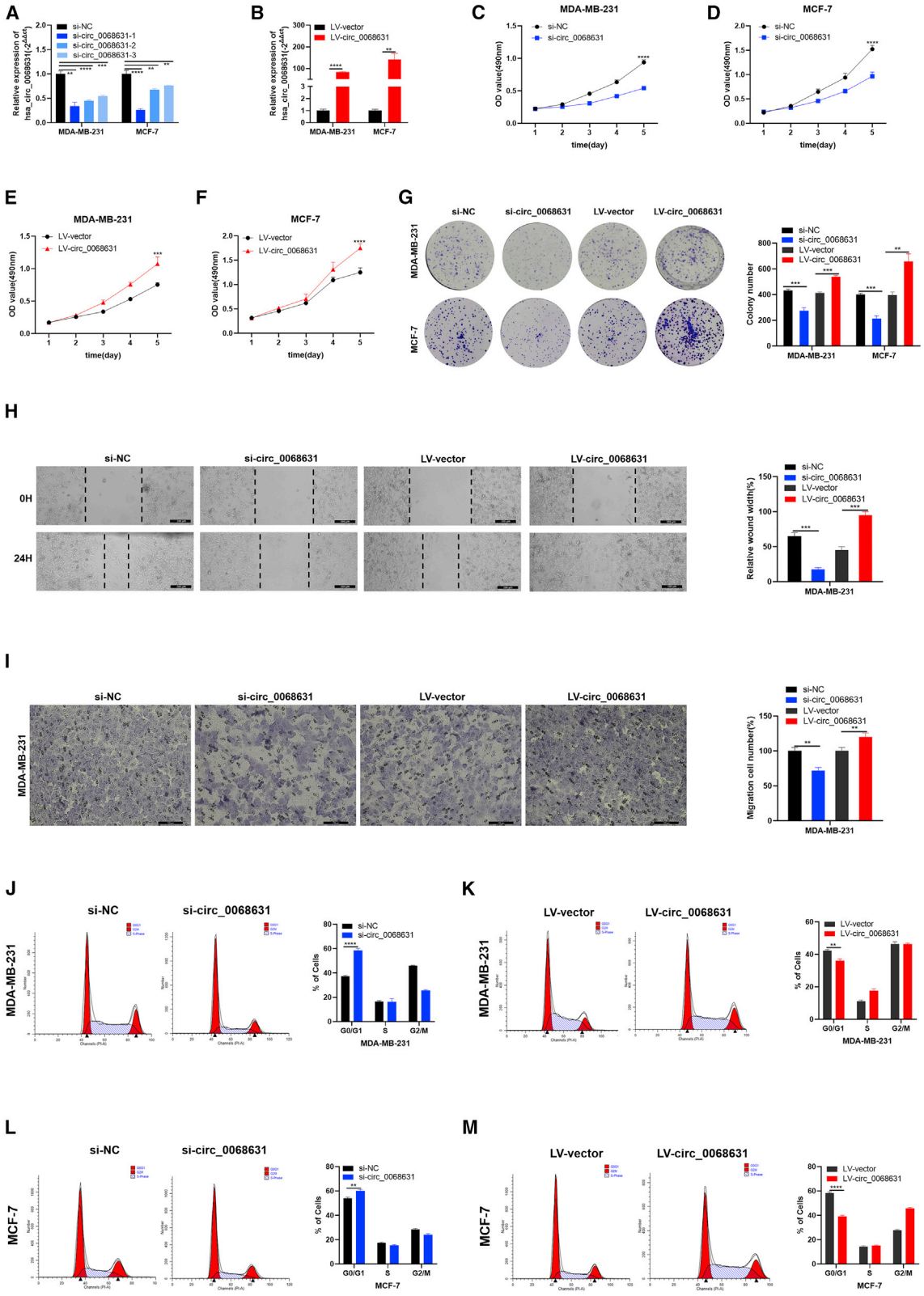

(legend on next page)

A

Circular RNA	Tag Name	% Identity	Alignment Length	Mismatches	Gap Openings	Tag Start	Tag End	Circular RNA Start	Circular RNA ENd
hsa_circ_0068631 Length: 261 nt	HHLE1_257438_eIF4AIII_rep1_257438_61_203	100.00	203	0	0	1	203	-201	+2
hsa_circ_0068631 Length: 261 nt	HHLE2_855312_eIF4AIII_rep2_855312_108_204	100.00	204	0	0	1	204	-202	+2

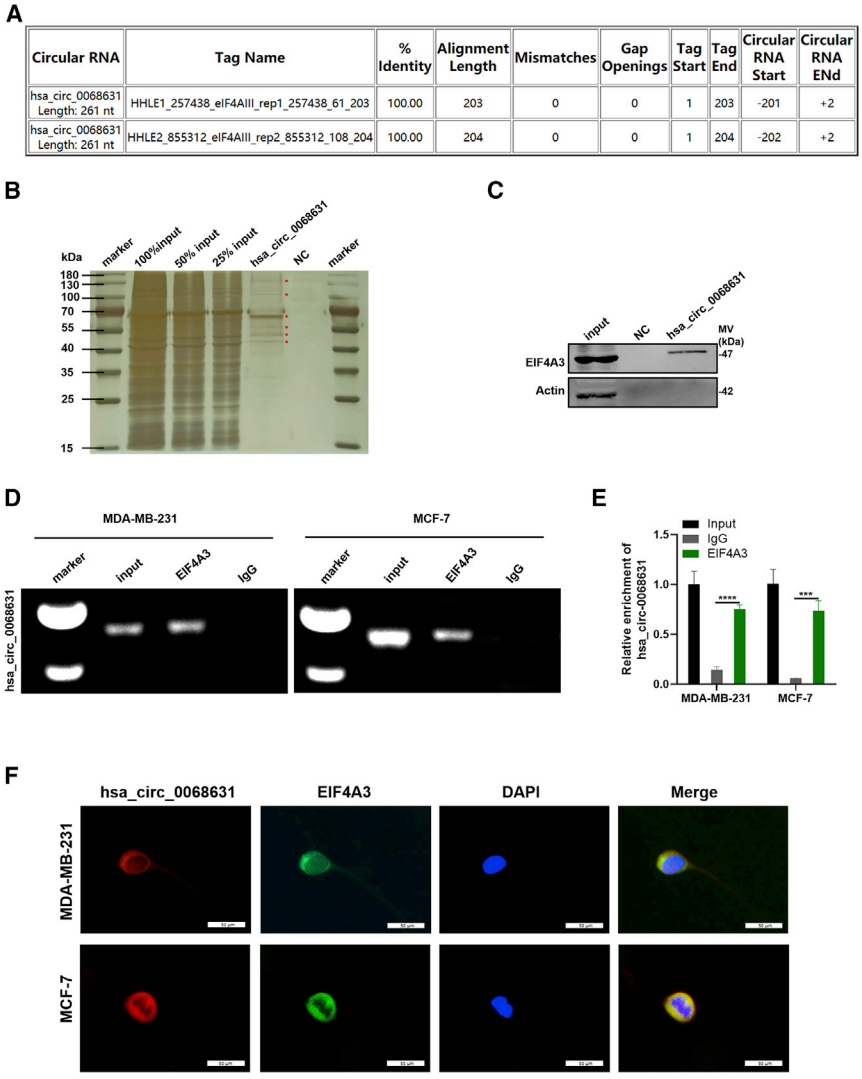

Figure 3. hsa_circ_0068631 could bind to EIF4A3

(A) Potential binding site between EIF4A3 and hsa_circ_0068631 according to CircInteractome. (B) Pull-down silver staining was used to demonstrate the potential RBPs binding to hsa_circ_0068631. (C) Interaction between EIF4A3 and hsa_circ_0068631 was demonstrated by an RNA pull-down assay. (D and E) An anti-EIF4A3 RIP assay was applied to validate the binding of EIF4A3 to hsa_circ_0068631. (F) An IF/FISH assay showed the location of hsa_circ_0068631and EIF4A3 in BC cells (scale bars, 50 μm).

pathway was enriched among EIF4A3 co-expressed partners.[12] Through TCGA database, we found that the expression of EIF4A3 was also positively correlated with c-Myc (Figure S1I). Then, we investigated c-Myc expression in BC tissues by quantitative real-time PCR, and c-Myc was significantly overexpressed in BC tissues (Figures 5A and 5B). Pearson's correlation analysis demonstrated the expression of hsa_circ_0068631 was positively correlated with c-Myc (Figure 5C). Then, we intended to examine the potential regulatory effect of hsa_circ_0068631 on c-Myc. We detected the mRNA and protein levels of c-Myc in BC cells transfected with si-circ_0068631 or LV-circ_0068631. Of note, the protein levels of c-Myc were positively regulated by hsa_circ_0068631, but the mRNA levels of c-Myc had no changes (Figures 5D and 5F). More importantly, we found that c-Myc protein levels were upregulated in both the nucleus and cytoplasm component with hsa_circ_0068631 overexpression (Figure 5F). Therefore, we assumed that hsa_circ_0068631 regulates c-Myc at the post-transcriptional level through recruiting EIF4A3. Thereafter, we conducted a RIP assay to validate the binding of EIF4A3 to c-Myc mRNA (Figure 5G). Furthermore, the enrichment of c-Myc mRNA in anti-EIF4A3 precipitates was decreased due to hsa_circ_0068631 depletion (Figures 5H–5I). Then, we added actinomycin D to BC cells treated with si-circ_0068631 and siRNA targeting human EIFA43 (si-EIF4A3), respectively, to test the mRNA stability of c-Myc. As expected, c-Myc mRNA stability was reduced due to hsa_circ_0068631 depletion or EIF4A3 depletion (Figure 5J, 5K, 5M, and 5N). Furthermore, EIF4A3 overexpression rescued the c-Myc mRNA stability decrease induced by hsa_circ_0068631 depletion in BC cells (Figures 5L and 5O). Given that cyclin E and CDK4 were confirmed target genes of c-Myc,[13,14] we further examined c-Myc stabilization through detecting cyclin E and CDK4 protein levels in hsa_circ_0068631 depletion and overexpression BC cells. As shown in Figure 5P, both cyclin E and CDK4 protein levels were positively regulated by hsa_circ_0068631. To further confirm that hsa_circ_0068631 maintains the stability of

Figure 2. hsa_circ_0068631 exerted an oncogenic role in BC cells

(A) Expression of hsa_circ_0068631 was confirmed by quantitative real-time PCR in BC cells transfected with si-NC or si-circ_0068631. (B) Expression of hsa_circ_0068631 was confirmed by quantitative real-time PCR in BC cells transfected with LV-vector or LV-circ_0068631. (C–F) Effect of si-circ_0068631 and LV-circ_0068631 on proliferation in BC cell lines by an MTT assay. (G) Effect of si-circ_0068631 and LV-circ_0068631 on proliferation in BC cell lines by a colony formation assay. (H) Wound-healing assays were performed in MDA-MB-231 cells treated with si-circ_0068631 or LV-circ_0068631 (scale bars, 200 μm). (I) Cell migration assays were performed in MDA-MB-231 cells treated with si-circ_0068631 or LV-circ_0068631 (scale bars, 100 μm). (J–M) Cell cycle assays were performed in BC cells treated with si-circ_0068631 or LV-circ_0068631. $^{**}p < 0.01$, $^{***}p < 0.001$, $^{****}p < 0.0001$.

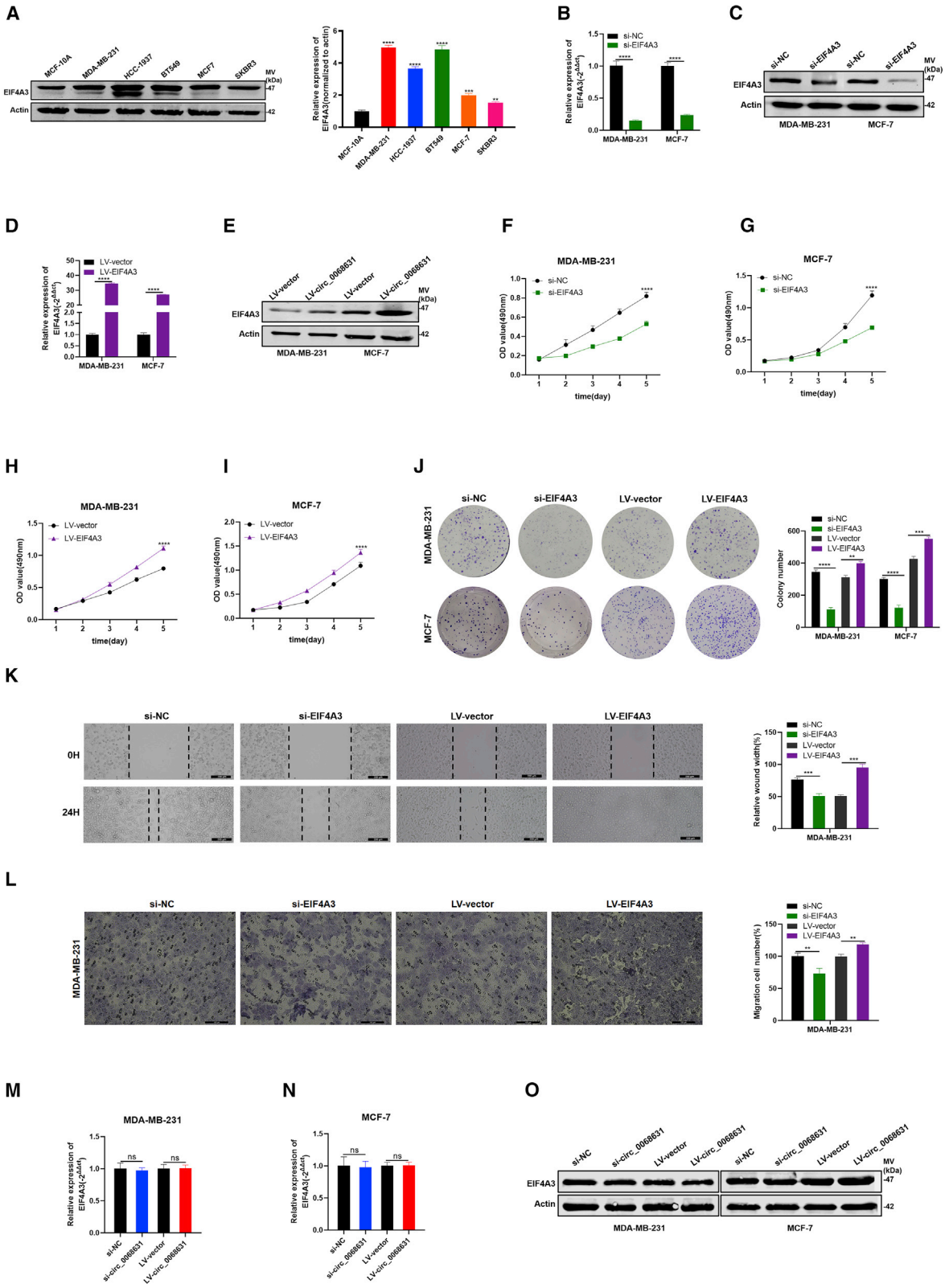

(legend on next page)

c-Myc mRNA by recruiting EIF4A3, we examined the changes of c-Myc protein in BC cells with EIF4A3 knocked down. As expected, the upregulating effect of hsa_circ_0068631 on c-Myc markedly decreased due to EIF4A3 depletion (Figure 5Q). In conclusion, these findings revealed that hsa_circ_0068631 enhanced c-Myc mRNA stability through recruiting EIF4A3.

Depletion of c-Myc rescued the promotive effect of hsa_circ_0068631 overexpression on biological activities in BC

Eventually, rescue assays were carried out to explore whether hsa_circ_0068631 affected the tumorigenesis of BC through c-Myc. MDA-MB-231 and MCF-7 cells were co-transfected with siRNA targeting c-Myc (si-c-Myc) and LV-circ_0068631. MTT and colony formation assays manifested that cell proliferation promoted by LV-circ_0068631 was hindered by si-c-Myc (Figures 6A–6C). Furthermore, c-Myc attenuation decreased MDA-MB-231 cell migration promoted by hsa_circ_0068631 overexpression (Figure 6D). In addition, the upregulation of c-Myc protein levels under hsa_circ_0068631 overexpression was recovered by si-c-Myc (Figure 6E). In summary, depletion of c-Myc rescued the promotive effect of hsa_circ_0068631 overexpression on BC progression, confirming that hsa_circ_0068631 facilitates BC tumorigenesis through c-Myc.

Xenograft assay identified oncogenic role of hsa_circ_0068631 in BC

To further confirm the role of hsa_circ_0068631 *in vivo*, we carried out a xenograft tumor assay in MDA-MB-231 cells stably infected by LV-circ_0068631 or LV-vector (Figure 7A). 5 weeks later, mice tumors were collected, photographed, measured, and weighed. Not surprisingly, we found that hsa_circ_0068631 overexpression markedly increased the tumor volume and weight compared with the control group (Figures 7B–7D). Moreover, the xenograft tumor protein was extracted and the expression of c-Myc was detected by western blotting and immunohistochemistry (IHC) (Figures 7E–7F), indicating that hsa_circ_0068631 overexpression could upregulate the c-Myc protein level. Results of the xenograft assay supported the oncogenic role of hsa_circ_0068631 in BC. The mechanism of the hsa_circ_0068631/EIF4A3/c-Myc axis in BC is shown in Figure 7G.

DISCUSSION

In recent years, increasing evidence has illustrated that circRNAs play crucial oncogenic or anti-cancer roles in multiple cancers, including BC. Different from other noncoding RNAs such as long noncoding RNAs and microRNAs (miRNAs), the stable structure of covalently closed loops provides circRNAs with the ability to resist environmental degradation.[15–17]

In this study, we identified that a novel circRNA, hsa_circ_0068631, was remarkably upregulated in BC tissues and cell lines. Of note, abnormally high expression of hsa_circ_0068631 was positively related to the clinical pathological variables in 60 BC patients, such as TNM stage, tumor size, lymph node metastasis, and distant metastasis. Then, we verified that hsa_circ_0068631 could facilitate BC tumorigenesis *in vivo* and *in vitro*, indicating its function as a valuable therapeutic target for BC treatment.

Until now, circRNAs have been identified to participate in tumorigenesis through several mechanisms, such as sponging miRNAs,[18,19] binding to RBPs,[20–22] and regulating gene transcription[23,24] and translation.[25–28] Previous studies mainly focused on circRNAs serving as miRNA sponges. Actually, circRNAs could also competitively bind to and interact with RBPs.[29]

In our study, we found that hsa_circ_0068631 has a potential binding site with EIF4A3. EIF4A3 is a core component of the exon junction complex (EJC), playing significant roles in mRNA splicing, location, transport, translation, and degradation.[30–32] As a RBP, EIF4A3 has been reportedly implicated in interacting with RNAs and is considered as a diagnostic marker or therapeutic target for several cancers. For example, EIF4A3 could promote circMMP9 expression through binding circMMP9 mRNA transcript in the upstream region.[33] circ_cse1l inhibits colorectal cancer proliferation by binding to EIF4A3.[34] In BC, EIF4A3 was remarkably overexpressed and EIF4A3 overexpression was associated with poor prognosis,[12] indicating that EIF4A3 plays a key role in BC progression. Based on previous reports, c-Myc was enriched among EIF4A3 co-expressed partners.[12] c-Myc was significantly associated with cell death, proliferation, differentiation, stress pathways, and mechanisms of drug resistance, and activation of c-Myc has been widely reported in BC progression.[35] Many studies have focused on molecules that directly target c-Myc, which will provide invaluable potential anti-cancer therapeutic targets.[36]

According to TCGA database as well as our experimental results, c-Myc was upregulated in BC and positively correlated with hsa_circ_0068631. Of note, protein level rather than mRNA level of c-Myc was affected by hsa_circ_0068631. The RNA pull-down assay and RIP assay were performed to reveal that EIF4A3 could interact

Figure 4. EIF4A3 exerted an oncogenic role in BC cells

(A) EIF4A3 was highly expressed in BC cells compared with MCF-10A cells as confirmed by western blotting. (B) Expression of EIF4A3 was confirmed by quantitative real-time PCR in BC cells transfected with si-NC or si-EIF4A3. (C) Expression of EIF4A3 was confirmed by western blotting in BC cells transfected with si-NC or si-EIF4A3. (D) Expression of EIF4A3 was confirmed by quantitative real-time PCR in BC cells transfected with LV-vector or LV-EIF4A3. (E) Expression of EIF4A3 was confirmed by western blotting in BC cells transfected with LV-vector or LV-EIF4A3. (F–I) Effect of si-EIF4A3 or LV-EIF4A3 on proliferation in BC cell lines by an MTT assay. (J) Effect of si-EIF4A3 or LV-EIF4A3 on proliferation in BC cell lines by a colony formation assay. (K) Wound-healing assays were performed in MDA-MB-231 cells treated with si-EIF4A3 or LV-EIF4A3 (scale bars, 200 μm). (L) Cell migration assays were performed in MDA-MB-231 cells treated with si-EIF4A3 or LV-EIF4A3 (scale bars, 100 μm). (M and N) The mRNA level of EIF4A3 was evaluated in BC cells transfected with si-circ_0068631 or LV-circ_0068631. (O) The protein level of EIF4A3 was evaluated in BC cells transfected with si-circ_0068631 or LV-circ_0068631. $^{**}p < 0.01$, $^{***}p < 0.001$, $^{****}p < 0.0001$.

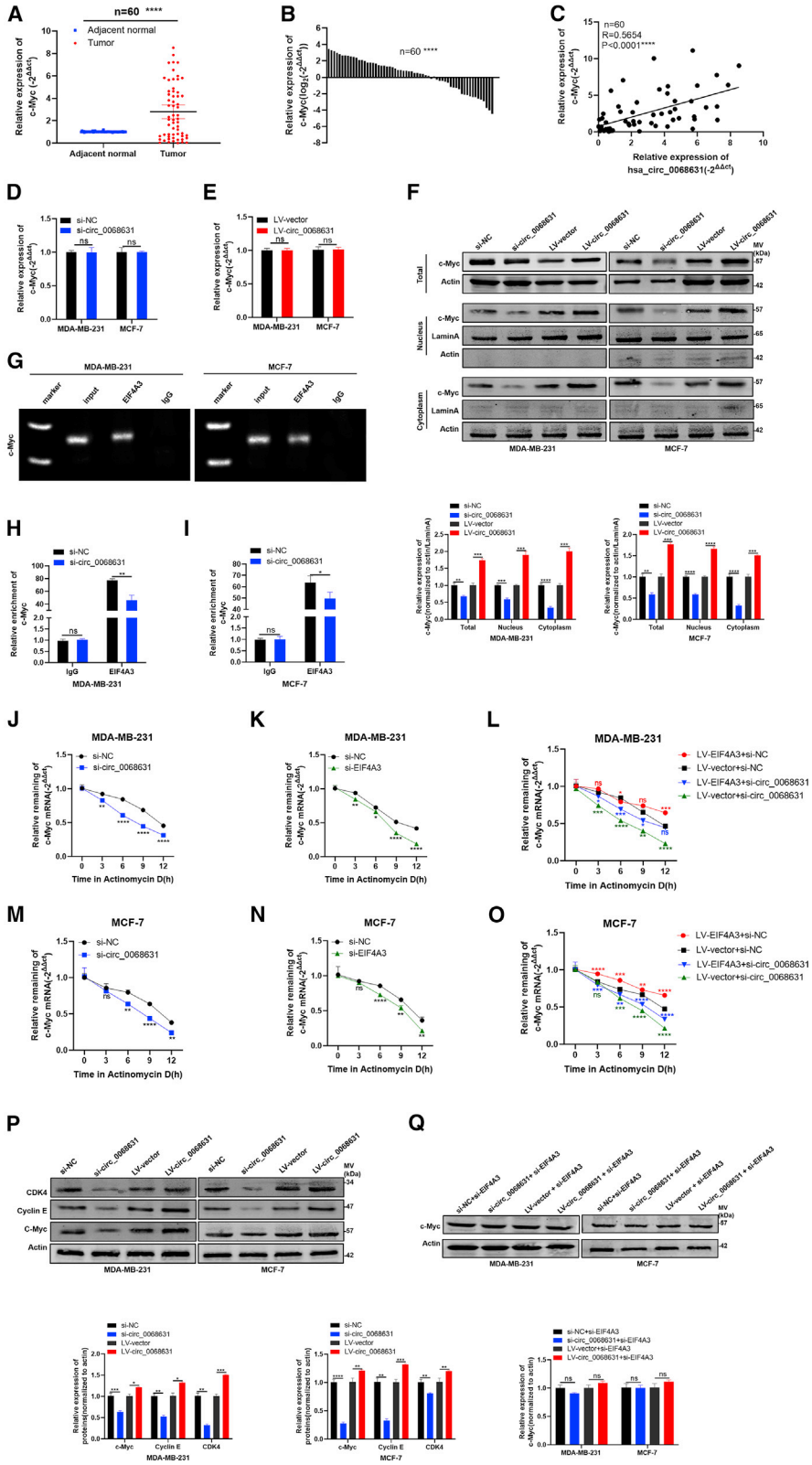

(legend on next page)

with hsa_circ_0068631 and c-Myc mRNA. In addition, hsa_circ_0068631 depletion reduced the interaction between EIF4A3 and c-Myc mRNA. Based on previous reports, RBPs can directly bind to RNA and play a pivotal part in the post-transcriptional process.[37] Thus, we supposed that hsa_circ_0068631 affected c-Myc mRNA stability via recruiting EIF4A3. Through an actinomycin D assay, we confirmed that the mRNA stability of c-Myc was influenced by hsa_circ_0068631 and EIF4A3. Eventually, we conducted rescue assays and further verified that depletion of c-Myc could invert the promotive effect of hsa_circ_0068631 overexpression on biological activities in BC.

In conclusion, our study demonstrated that upregulation of hsa_circ_0068631 could facilitate the progression of BC by binding to EIF4A3 to maintain c-Myc mRNA stability. Suppressing the hsa_circ_0068631/EIF4A3/c-Myc axis represents a potential strategy for BC.

MATERIALS AND METHODS

Clinical tissue samples

In total, 60 tumor tissues and paired adjacent normal tissues of BC patients were collected from the Department of Breast and Thyroid Surgery of Shanghai Tenth People's Hospital (Shanghai, China) from 2017 to 2020. Patients who received radiotherapy, chemotherapy, or any other neoadjuvant therapy before surgery were excluded. All excised specimens were rapidly stored in liquid nitrogen. Clinical characteristics of all patients were recorded. This study was approved by Institutional Ethics Committee of Shanghai Tenth People's Hospital. Informed consent was signed by all patients.

Cell culture and transfection

All cell lines involved in this study were purchased from the Chinese Academy of Sciences (Shanghai, China). BC cell lines and HEK293T cell line were cultured in Dulbecco's modified Eagle's medium (DMEM) (Gibco, USA) containing 10% fetal bovine serum (FBS) (Gibco, USA). Non-malignant breast epithelial cell line MCF-10A cells were cultured in mammary epithelial basal medium (MEBM) (Cambrex, USA). All cell lines were cultured in a CO_2 incubator at constant temperature. The si-circ_0068631 junction site, si-EIF4A3, and siRNA targeting the negative control (si-NC) were purchased from Generay Biotech (Shanghai, China). LV-circ_0068631 and LV-vector were purchased from QiheBio (Shanghai, China). We used Hieff Trans liposomal transfection reagent (Yeasen Biotechnology, China) for transfection according to the manufacturer's instructions.

RNA extraction and quantitative real-time PCR

Total RNA was isolated by TRIzol reagent (Invitrogen, USA). Hifair III first-strand cDNA synthesis SuperMix (Yeasen Biotechnology, China) was used to reverse RNA into cDNA. Hieff qPCR SYBR Green master mix (Yeasen Biotechnology, China) was used for quantitative real-time PCR. Data were normalized to GAPDH/U6/18S and quantified by the $2^{-\Delta\Delta Ct}$ method. Primer sequences were synthesized by Generay Biotech (Shanghai, China). Primers used in this study are shown in Table S1.

Confirming specificity for hsa_circ_0068631

PCR products amplified by hsa_circ_0068631 primers were separated on 1% agarose gel. Sanger sequencing was performed to validate the back-splicing junction site of hsa_circ_0068631.

RNase R resistance assay

MDA-MB-231 and MCF-7 cell lines were treated with RNase R (4 U/mg, Epicenter) and incubated for 30 min at 37°C. Then, the treated RNAs were reverse transcribed with specific primers and detected by a quantitative real-time PCR assay.

Actinomycin D assay

MDA-MB-231 and MCF-7 cells were treated with 2 mg/mL actinomycin D (Merck, Germany) to block transcription. Then, the remaining RNAs extracted from treated cells were assessed by qRT-PCR.

Subcellular fractionation

Nuclear and cytoplasmic extraction reagents (Thermo Fisher Scientific) were used for subcellular fractionation of BC cells. We used U6 as the nuclear control and GAPDH as the cytoplasmic control.

FISH

A Ribo FISH kit (Ribo, China) was used for the FISH assay. Specific probes for hsa_circ_0068631 were synthesized by RiboBio (Guangzhou, China). MDA-MB-231 and MCF-7 cells were fixed with 4% paraformaldehyde, treated with 0.5% Triton X-100, and incubated with a hsa_circ_0068631 probe overnight. Then, cell nuclei were stained with DAPI. Images were obtained with a fluorescence microscope (Olympus BX53 biological microscope).

IF

MDA-MB-231 and MCF-7 cells were fixed with 4% paraformaldehyde, treated with 0.5% Triton X-100, and immunoblotted overnight at 4°C with primary antibodies, i.e., anti-EIF4A3 (ABclonal, China). Then, the cells were incubated with secondary antibodies/Alexa Fluor

Figure 5. hsa_circ_0068631 regulated c-Myc through recruiting EIF4A3 at the post-transcriptional level

(A and B) c-Myc was highly expressed in tumor tissues compared with adjacent normal tissues. (C) Correlations between the expression of hsa_circ_0068631 and c-Myc were found with Pearson's correlation analysis in BC tissue samples (n = 60). (D and E) The mRNA level of c-Myc was evaluated in BC cells transfected with si-circ_0068631 or LV-circ_0068631. (F) The protein level of c-Myc was evaluated in BC cells transfected with si-circ_0068631 or LV-circ_0068631. (G) An anti-EIF4A3 RIP assay was applied to validate the binding of EIF4A3 to c-Myc. (H and I) The effect of hsa_circ_0068631 knockdown on the binding of EIF4A3 to c-Myc was assessed by a RIP assay. (J–O) After actinomycin D treatment, the mRNA stability of c-Myc in BC cells was determined by quantitative real-time PCR. (P) The protein levels of c-Myc target genes were evaluated in BC cells transfected with si-circ_0068631 or LV-circ_0068631. (Q) The protein level of c-Myc was evaluated in BC cells with EIF4A3 depletion. *$p < 0.05$, **$p < 0.01$, ****$p < 0.0001$.

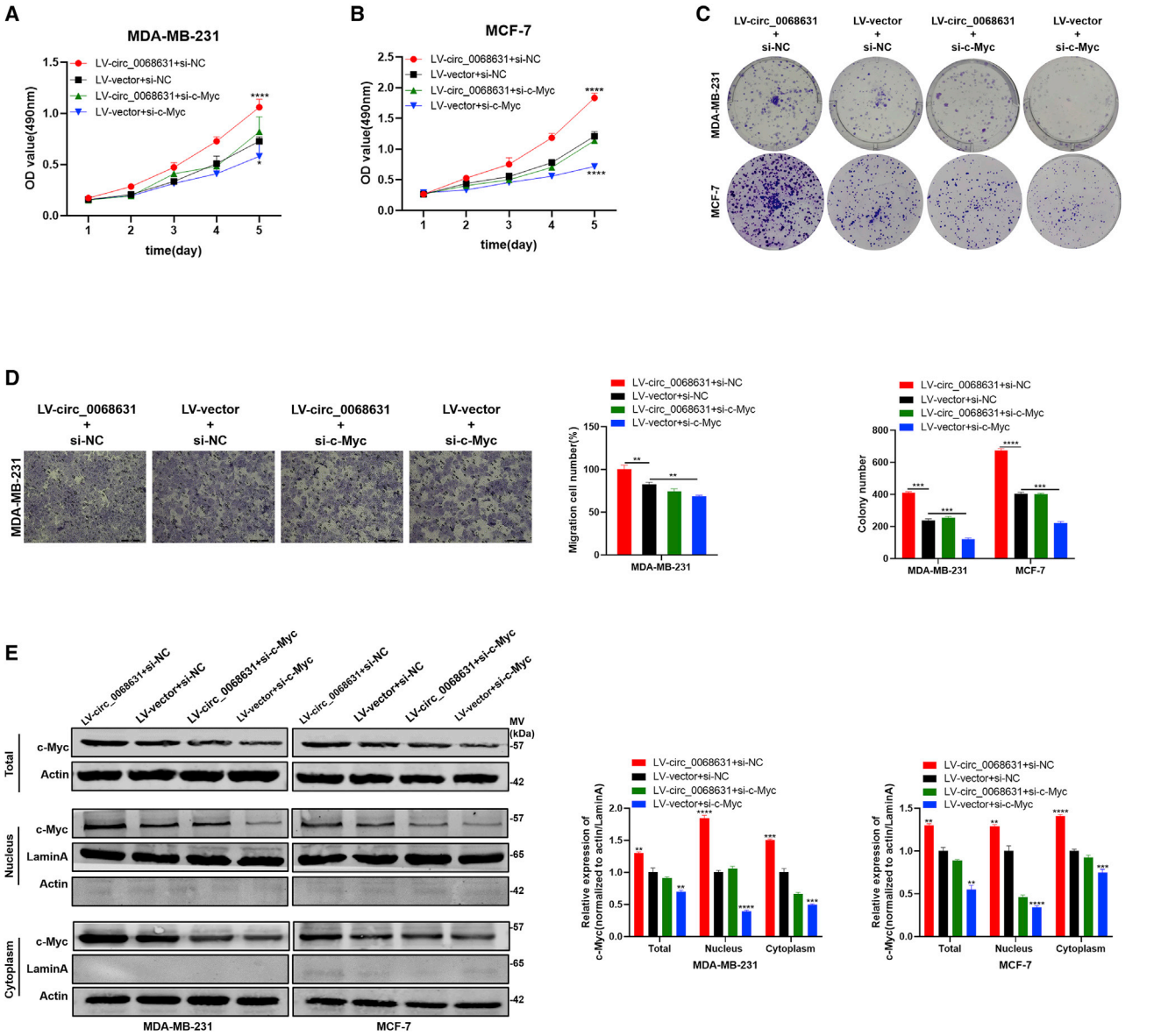

Figure 6. Depletion of c-Myc rescued the promotive effect of hsa_circ_0068631 overexpression on biological activities in BC

(A and B) si-c-Myc rescued the promotive effects of LV-circ_0068631 on BC cells by an MTT assay. (C) si-c-Myc rescued the promotive effects of LV-circ_0068631 on BC cells by a colony formation assay. (D) si-c-Myc rescued the promotive effects of LV-circ_0068631 on BC cells by a cell migration assay (scale bars, 100 μm). (E) si-c-Myc rescued the high expression of c-Myc caused by LV-circ_0068631 by western blotting. *p < 0.05, **p < 0.01, ***p < 0.001, ****p < 0.0001.

488 for 1 h at room temperature. Then, cell nuclei were stained with DAPI. Images were obtained with a fluorescence microscope (Olympus BX53 biological microscope).

MTT assay

Transfected BC cells at a density of 2,000 were seeded in 96-well plates. An MTT assay kit (Sigma, USA) was used to detect living cells. The absorbance at 490 nm was measured by a microplate reader at five time periods (0, 24, 48, 72, and 96 h).

Colony formation assay

Transfected BC cells at a density of 1,000 were seeded in six-well plates. Cell colonies were subsequently washed, fixed, and stained until the colonies were visible. Then, colonies were counted and imaged.

Wound-healing assay

Transfected BC cells were seeded in six-well plates. A scratch was produced over the cells with a 200-μL pipette tip, and detached cells were removed by washing with PBS. All cells used in the wound-healing

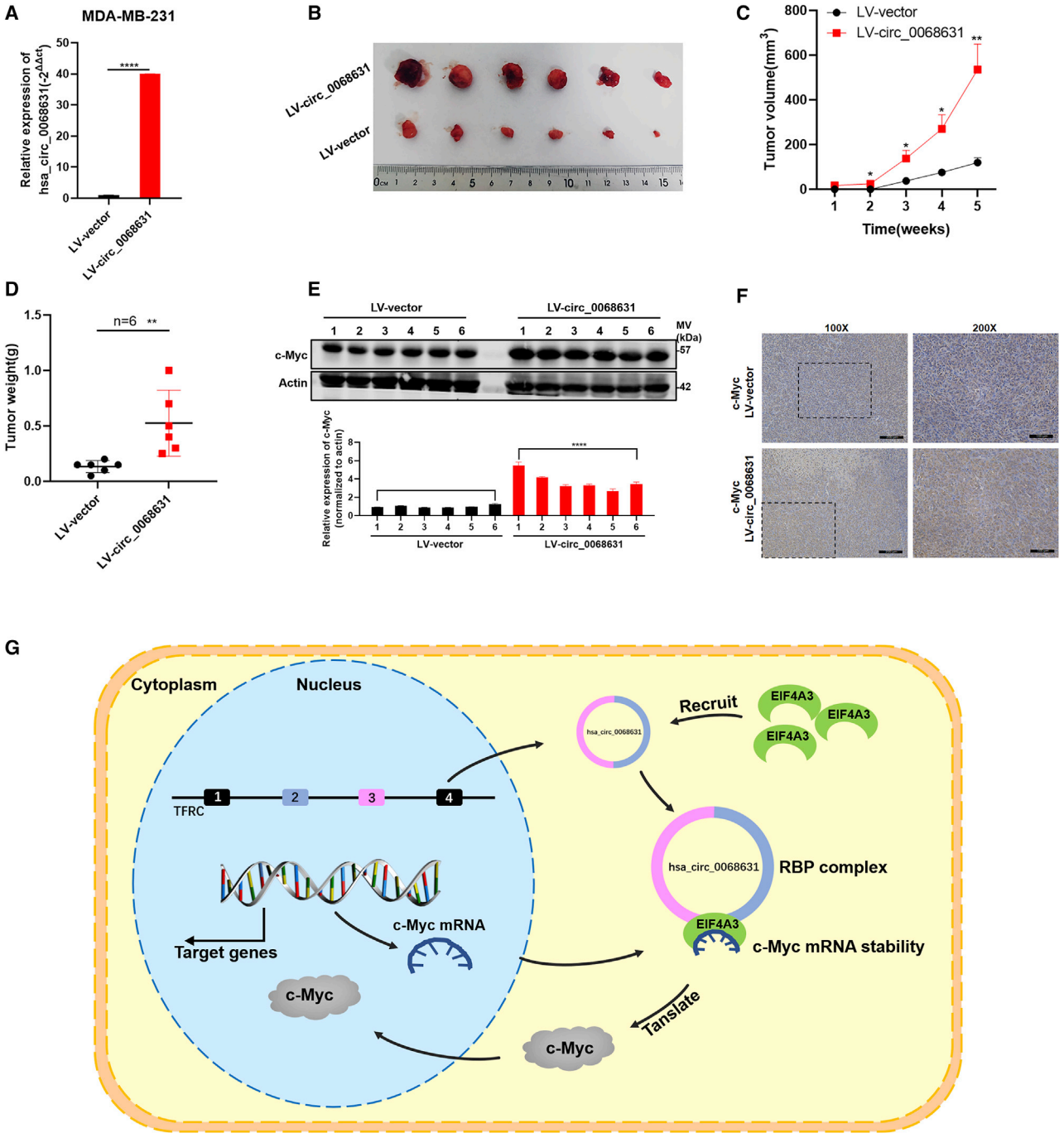

Figure 7. Xenograft assay identified the oncogenic role of hsa_circ_0068631 in BC

(A) Expression of hsa_circ_0068631 was confirmed by quantitative real-time PCR in BC cells transfected with LV-vector or LV- circ_0068631. (B) Representative images of xenograft tumors in nude mice. (C) The growth curves of xenografts. (D) Average tumor weight of nude mice. (E) The expression level of c-Myc in xenograft tumors was measured by western blotting. (F) Immunohistochemistry (IHC) staining of c-Myc in xenografts (left, scale bars, 200 μm; right, scale bars, 100 μm). (G) The mechanism diagram was generated to illustrate the hsa_circ_0068631/EIF4A3/c-Myc axis in BC. *p < 0.05, **p < 0.01, ****p < 0.0001.

assay were cultured with DMEM with 2% FBS. The area of each scratch was assessed with a microscope at 0 and 24 h for the MDA-MB-231 cell line and at 0 and 48 h for the MCF-7 cell line.

Transwell assay

Transfected BC cells were added into the upper chamber with 200 μL of serum-free medium, and medium with 10% FBS was added into the

lower chamber. After culturing for 16 h for the MDA-MB-231 cell line and 30 h for the MCF-7 cell line, cells that migrated to the opposite side of the filter were fixed, stained, imaged (Leica Microsystems, Germany), and counted.

Flow cytometry assay

Transfected BC cells were harvested and fixed in ice-cold ethanol for more than 4 h. Then 0.5 mL of 0.05 mg/mL propidium iodide (PI) staining solution was added into cell samples. After incubating for 30 min at 37°C, the cell cycle was analyzed by flow cytometer (FACSCanto II, BD Biosciences).

RNA pull-down assay

A BersinBio RNA pull-down kit (BersinBio, Guangzhou, China) was adopted for detecting related RBPs of hsa_circ_0068631. The biotin-labeled probe targeting the junction site of hsa_circ_0068631 was designed and synthesized by GenePharma (Shanghai, China). Through incubation of specific probes with cell lysates, the RNA-protein complex was formed. Then, the complex was isolated by streptavidin-conjugated magnetic beads. After being separated by 10% polyacrylamide gel electrophoresis (PAGE), the related RBPs of hsa_circ_0068631 were stained by silver, followed by a western blotting assay.

RIP assay

A BersinBio RIP assay kit (BersinBio, Guangzhou, China) was used for RIP assays. Cell lysates were incubated with magnetic beads and anti-EIF4A3 (Proteintech, China) or anti-IgG (ABclonal, China). The enriched RNAs were analyzed by quantitative real-time PCR.

Western blotting analysis

Total proteins were extracted by using RIPA lysis buffer (Beyotime, Jiangsu, China). Protein lysates were separated by 10% SDS-PAGE gels and then transferred to a nitrocellulose membrane (Beyotime, Jiangsu, China). After incubation with 5% non-fat milk for more than 1 h to block nonspecific binding, the membranes were immunoblotted overnight at 4°C with primary antibodies, i.e., anti-EIF4A3 (Proteintech, USA), anti-c-Myc (Proteintech, USA), anti-cyclin E (Abcam, USA), anti-CDK4 (Abcam, USA), anti-TFRC (ABclonal, China) anti-Lamin A (Proteintech, USA) and anti-β-actin (ABclonal, China). Then, the membranes were incubated with diluted secondary antibodies for 1 h at room temperature. The membranes were scanned by an Odyssey infrared scanning system (LI-COR Biosciences, Lincoln, NE, USA).

Xenograft tumor assay

Transfected MDA-MB-231 cells with LV-circ_0068631 or LV-vector were injected into the second mammary fat pad of 4-week-old female athymic nude mice (n = 6, each group). Tumor growth was monitored every week. 6 weeks later, all mice were killed by cervical dislocation. The collected tumors volumes were measured and calculated according to (width2 × length)/2. All experimental and animal care procedures complied with the rules of the Ethics Committee of Shanghai Tenth People's Hospital of Tongji University.

IHC

Fresh tumor samples were embedded in paraffin and then sectioned into 4-μm slices. The slices were incubated with anti-c-Myc (Proteintech, USA), counterstained with hematoxylin (Sigma-Aldrich), and imaged with a microscope (Leica Microsystems, Mannheim, Germany).

Statistical analysis

Data analysis was performed by GraphPad Prism v8.0 (GraphPad, CA, USA). Means ± standard deviation (SD) of results were obtained from three independent experiments. The significance of differences between groups were analyzed with the Student's t test, and $p < 0.05$ was considered significant.

SUPPLEMENTAL INFORMATION

Supplemental information can be found online at https://doi.org/10.1016/j.omtn.2021.07.003.

ACKNOWLEDGMENTS

This work was supported by grants from the National Natural Science Foundation of China (no. 82073204) and the Shanghai Municipal Health Commission (no. 202040157). We thank the Department of Thyroid and Breast Surgery, Shanghai Tenth People's Hospital, Shanghai, China, for providing the BC tissue samples and related anonymous clinical data. The authors would like to acknowledge the helpful comments on this paper received from the reviewers.

AUTHOR CONTRIBUTIONS

X.W. and L.F. designed the research. X.W. and M.C. performed the research and analyzed results. X.W. wrote the paper. All authors read and approved the final manuscript.

DECLARATION OF INTERESTS

The authors declare no competing interests.

REFERENCES

1. Siegel, R.L., Miller, K.D., and Jemal, A. (2020). Cancer statistics, 2020. CA Cancer J. Clin. *70*, 7–30.
2. Siegel, R.L., Miller, K.D., and Jemal, A. (2019). Cancer statistics, 2019. CA Cancer J. Clin. *69*, 7–34.
3. Wang, X., and Fang, L. (2018). Advances in circular RNAs and their roles in breast cancer. J. Exp. Clin. Cancer Res. *37*, 206.
4. Geng, Z., Wang, W., Chen, H., Mao, J., Li, Z., and Zhou, J. (2019). circ_0001667 promotes breast cancer cell proliferation and survival via Hippo signal pathway by regulating TAZ. Cell Biosci. *9*, 104.
5. Xu, J.H., Wang, Y., and Xu, D. (2019). hsa_circ_001569 is an unfavorable prognostic factor and promotes cell proliferation and metastasis by modulating PI3K-AKT pathway in breast cancer. Cancer Biomark. *25*, 193–201.
6. Li, Y., Zheng, Q., Bao, C., Li, S., Guo, W., Zhao, J., Chen, D., Gu, J., He, X., and Huang, S. (2015). Circular RNA is enriched and stable in exosomes: A promising biomarker for cancer diagnosis. Cell Res. *25*, 981–984.
7. Chen, L.L. (2016). The biogenesis and emerging roles of circular RNAs. Nat. Rev. Mol. Cell Biol. *17*, 205–211.
8. Vea, A., Llorente-Cortes, V., and de Gonzalo-Calvo, D. (2018). Circular RNAs in blood. Adv. Exp. Med. Biol. *1087*, 119–130.

9. Sparano, J.A., Gray, R.J., Makower, D.F., Pritchard, K.I., Albain, K.S., Hayes, D.F., Geyer, C.E., Jr., Dees, E.C., Perez, E.A., Olson, J.A., Jr., et al. (2015). Prospective validation of a 21-gene expression assay in breast cancer. N. Engl. J. Med. *373*, 2005–2014.

10. McNeill, R.E., Miller, N., and Kerin, M.J. (2007). Evaluation and validation of candidate endogenous control genes for real-time quantitative PCR studies of breast cancer. BMC Mol. Biol. *8*, 107.

11. Majidzadeh-A, K., Esmaeili, R., and Abdoli, N. (2011). TFRC and ACTB as the best reference genes to quantify urokinase plasminogen activator in breast cancer. BMC Res. Notes *4*, 215.

12. Lin, Y., Zhang, J., Cai, J., Liang, R., Chen, G., Qin, G., Han, X., Yuan, C., Liu, Z., Li, Y., et al. (2018). Systematic analysis of gene expression alteration and co-expression network of eukaryotic initiation factor 4A-3 in cancer. J. Cancer *9*, 4568–4577.

13. Zhou, Y., Geng, Y., Zhang, Y., Zhou, Y., Chu, C., Sharma, S., Fassl, A., Butter, D., and Sicinski, P. (2020). The requirement for cyclin E in c-Myc overexpressing breast cancers. Cell Cycle *19*, 2589–2599.

14. Mateyak, M.K., Obaya, A.J., and Sedivy, J.M. (1999). c-Myc regulates cyclin D-Cdk4 and -Cdk6 activity but affects cell cycle progression at multiple independent points. Mol. Cell. Biol. *19*, 4672–4683.

15. Bach, D.H., Lee, S.K., and Sood, A.K. (2019). Circular RNAs in cancer. Mol. Ther. Nucleic Acids *16*, 118–129.

16. Ng, W.L., Mohd Mohidin, T.B., and Shukla, K. (2018). Functional role of circular RNAs in cancer development and progression. RNA Biol. *15*, 995–1005.

17. Li, J., Sun, D., Pu, W., Wang, J., and Peng, Y. (2020). Circular RNAs in cancer: Biogenesis, function, and clinical significance. Trends Cancer *6*, 319–336.

18. Hansen, T.B., Jensen, T.I., Clausen, B.H., Bramsen, J.B., Finsen, B., Damgaard, C.K., and Kjems, J. (2013). Natural RNA circles function as efficient microRNA sponges. Nature *495*, 384–388.

19. Militello, G., Weirick, T., John, D., Döring, C., Dimmeler, S., and Uchida, S. (2017). Screening and validation of lncRNAs and circRNAs as miRNA sponges. Brief. Bioinform. *18*, 780–788.

20. Yang, Q., Du, W.W., Wu, N., Yang, W., Awan, F.M., Fang, L., Ma, J., Li, X., Zeng, Y., Yang, Z., et al. (2017). A circular RNA promotes tumorigenesis by inducing c-myc nuclear translocation. Cell Death Differ. *24*, 1609–1620.

21. Zeng, Y., Du, W.W., Wu, Y., Yang, Z., Awan, F.M., Li, X., Yang, W., Zhang, C., Yang, Q., Yee, A., et al. (2017). A circular RNA binds to and activates AKT phosphorylation and nuclear localization reducing apoptosis and enhancing cardiac repair. Theranostics *7*, 3842–3855.

22. Abdelmohsen, K., Panda, A.C., Munk, R., Grammatikakis, I., Dudekula, D.B., De, S., Kim, J., Noh, J.H., Kim, K.M., Martindale, J.L., and Gorospe, M. (2017). Identification of HuR target circular RNAs uncovers suppression of PABPN1 translation by *CircPABPN1*. RNA Biol. *14*, 361–369.

23. Holdt, L.M., Kohlmaier, A., and Teupser, D. (2018). Molecular roles and function of circular RNAs in eukaryotic cells. Cell. Mol. Life Sci. *75*, 1071–1098.

24. Verduci, L., Ferraiuolo, M., Sacconi, A., Ganci, F., Vitale, J., Colombo, T., Paci, P., Strano, S., Macino, G., Rajewsky, N., and Blandino, G. (2017). The oncogenic role of circPVT1 in head and neck squamous cell carcinoma is mediated through the mutant p53/YAP/TEAD transcription-competent complex. Genome Biol. *18*, 237.

25. Zheng, X., Chen, L., Zhou, Y., Wang, Q., Zheng, Z., Xu, B., Wu, C., Zhou, Q., Hu, W., Wu, C., and Jiang, J. (2019). A novel protein encoded by a circular RNA circPPP1R12A promotes tumor pathogenesis and metastasis of colon cancer via Hippo-YAP signaling. Mol. Cancer *18*, 47.

26. Xia, X., Li, X., Li, F., Wu, X., Zhang, M., Zhou, H., Huang, N., Yang, X., Xiao, F., Liu, D., et al. (2019). A novel tumor suppressor protein encoded by circular AKT3 RNA inhibits glioblastoma tumorigenicity by competing with active phosphoinositide-dependent kinase-1. Mol. Cancer *18*, 131.

27. Chen, C.Y., and Sarnow, P. (1995). Initiation of protein synthesis by the eukaryotic translational apparatus on circular RNAs. Science *268*, 415–417.

28. Yang, Y., Fan, X., Mao, M., Song, X., Wu, P., Zhang, Y., Jin, Y., Yang, Y., Chen, L.L., Wang, Y., et al. (2017). Extensive translation of circular RNAs driven by N^6-methyladenosine. Cell Res. *27*, 626–641.

29. Zang, J., Lu, D., and Xu, A. (2020). The interaction of circRNAs and RNA binding proteins: An important part of circRNA maintenance and function. J. Neurosci. Res. *98*, 87–97.

30. Saulière, J., Murigneux, V., Wang, Z., Marquenet, E., Barbosa, I., Le Tonquèze, O., Audic, Y., Paillard, L., Roest Crollius, H., and Le Hir, H. (2012). CLIP-seq of eIF4AIII reveals transcriptome-wide mapping of the human exon junction complex. Nat. Struct. Mol. Biol. *19*, 1124–1131.

31. Gehring, N.H., Lamprinaki, S., Kulozik, A.E., and Hentze, M.W. (2009). Disassembly of exon junction complexes by PYM. Cell *137*, 536–548.

32. Rocak, S., and Linder, P. (2004). DEAD-box proteins: The driving forces behind RNA metabolism. Nat. Rev. Mol. Cell Biol. *5*, 232–241.

33. Wang, R., Zhang, S., Chen, X., Li, N., Li, J., Jia, R., Pan, Y., and Liang, H. (2018). EIF4A3-induced circular RNA MMP9 (circMMP9) acts as a sponge of miR-124 and promotes glioblastoma multiforme cell tumorigenesis. Mol. Cancer *17*, 166.

34. Xu, B., Yang, N., Liu, Y., Kong, P., Han, M., and Li, B. (2020). circ_cse1l inhibits colorectal cancer proliferation by binding to eIF4A3. Med. Sci. Monit. *26*, e923876.

35. Fallah, Y., Brundage, J., Allegakoen, P., and Shajahan-Haq, A.N. (2017). MYC-driven pathways in breast cancer subtypes. Biomolecules *7*, 53.

36. Han, H., Jain, A.D., Truica, M.I., Izquierdo-Ferrer, J., Anker, J.F., Lysy, B., Sagar, V., Luan, Y., Chalmers, Z.R., Unno, K., et al. (2019). Small-molecule MYC inhibitors suppress tumor growth and enhance immunotherapy. Cancer Cell *36*, 483–497.e15.

37. Li, Q., Lei, C., Lu, C., Wang, J., Gao, M., and Gao, W. (2019). LINC01232 exerts oncogenic activities in pancreatic adenocarcinoma via regulation of TM9SF2. Cell Death Dis. *10*, 698.